A Cable-Driven Robotic Eye for Understanding Eye-Movement Control

1st Akhil John
Institute for Systems and Robotics
Instituto Superior Técnico
Lisbon, Portugal
akhil.john@tecnico.ulisboa.pt

2nd John Van Opstal
Section Neurophysics
Donders Centre for Neuroscience
Radbound University
Nijmegen, the Netherlands
John.vanOpstal@donders.ru.nl

3rd Alexandre Bernardino
Institute for Systems and Robotics
Instituto Superior Técnico
Lisbon, Portugal
alexandre.bernardino@tecnico.ulisboa.pt

***Abstract*—We propose a design for a bio-inspired robotic eye, with 6 independently controlled muscles, that is suitable for studying the emergence of human saccadic eye movements characteristics. Understanding how characteristics like the restriction of eye orientations to a 2D manifold, straight saccadic trajectories, and saturating relationship between saccade amplitude and its peak velocity come about in a highly nonlinear system with non-commutativity of rotations is not trivial. Although earlier studies have addressed some of these problems, none have so far considered the full 3D complexity of ocular kinematics and dynamics. Our design contains a spherical eye actuated by six motor-driven cables with realistic pulling directions to mimic the six extraocular muscles. The coupling between the eyeball and eye socket has been designed to specify a damped rotational system, which is key to understanding the signals involved in the control of artificial and biological eyes. We present the mechanical design of the robotic system and a simulation model based on it. The system has a large range of movement and its dynamical responses to step inputs are shown, thus illustrating its ability to perform a wide range of eye movements with the appropriate characteristics.**

***Index Terms*—Cable-driven robots; Bio-inspired robots; Eye-movements; Oculomotor system; Saccades.**

I. Introduction

The human visual system provides detailed information about the shapes, sizes, colors, locations, and movements of objects in the environment. Since high visual acuity is only present in the central two degrees of the visual field (the fovea), we need rapid and goal-directed eye movements to foveate at a selected target. Saccades are ballistic eye movements of the oculomotor system, reaching speeds up to about 700°/s. They enable quick re-fixation of a novel target of interest and serve to rapidly scan the environment for relevant targets.

Neurophysiology has shown that during saccades, the six extraocular muscles work in agonist-antagonist pairs [1]. Although mechanically the eye can rotate with three degrees of rotational freedom, behavioral recordings showed that when the head is held fixed and upright, Donders' Law restricts eye orientations during saccades, smooth pursuit, and vergence to a 2D manifold [2]. Moreover, when the eyes fixate, saccade to, or follow distant targets, Listing's Law dictates that this 2D manifold reduces to a plane.

Saccadic eye movements show stereotypical dynamical characteristics, known as the main sequence [3]: saccade duration increases as an affine relation with saccade amplitude and, consequently, the peak eye velocity saturates for large saccades. Furthermore, the saccade acceleration phase is largely independent of amplitude. Moreover, despite these nonlinear dynamics, saccade trajectories are approximately straight in all directions, which is due to a considerable amount of cross-coupling between the driving signals to the eye muscles. Characteristics such as these are used for diagnosing neurological disorders at higher cortical, cerebellar, or brainstem levels [4]. Even though these properties are well established and have been studied for decades [5], it is still not completely understood how saccades are programmed and controlled by the brain to drive the 3D oculomotor plant.

There exists a large body of knowledge about the mammalian oculomotor system, in particular concerning saccades, resulting from neuro-anatomical studies and single-unit neural recordings performed at many levels in the brains of trained macaque monkeys and cats. These findings have led to powerful computational neurobiological models for saccades and the underlying neural circuits [5]. Furthermore, the mechanical structures and biomechanics of the oculomotor plant have been well described and modeled, and are successfully used to guide strabismus surgeries [6], [7]. However, how the oculomotor plant behaves under dynamic conditions imposed by high-velocity saccades, is not well understood.

We believe that studying this problem with the aid of a realistic biomimetic robotic eye allows one to efficiently test different hypotheses, muscle properties, and system parameters, in order to better understand the neuro-biological system. This works both ways: a deeper understanding of the oculomotor system may lead to novel therapies to treat and alleviate eye-movement disorders, as well as to develop more efficient robotic visual systems.

In this paper, we discuss the design of a novel biomimetic robotic eye and the physics-based simulation model that is derived from it. Section II summarizes the relevant anatomical

Supported by LARSyS - FCT Project (UIDB/50009/2020), VOAMAIS (PTDC/EEI-AUT/31172/2017, 02/SAICT/2017/31172), and the European Commission project ORIENT (ERC/2016/693400)

details of the oculomotor plant. In section III, we review the existing literature, which leads to the motivation of our design requirements, discussed in section IV. A detailed description of the components and subsystem is given in section V. In section VI, the modeling of the system for simulation is explained. Some experimental results are shown in section VII and section VIII mentions the conclusions and possible future work.

II. Extra-ocular anatomy

The human eye is suspended in a bony cavity called the orbit and is surrounded by fatty tissues. The eye is approximately spherical with a diameter of 2.4 cm and the six contractile extraocular muscles (see fig. 1) attach to the eye's sclera. These muscles work in three antagonistic pairs to rotate the eye. The four recti originate at the annulus of Zinn at the orbit's posterior end, and they attach at different sections on the globe. The superior oblique starts near the annulus of Zinn and passes through the trochlea before reaching the eye, while the inferior oblique originates from the maxillary bone near the nose. Note that the eye-muscle insertions are not symmetrically organized around the eyeball (see Table II). In addition, the conical orbit points outward from the straight-ahead direction at approximately 23°. These anatomical features make the muscles' pulling actions asymmetric and highly coupled. The resulting effect of pulling each muscle when the eye is looking straight ahead is described in Table I. The viscous fat around the eye, through which the optic nerve is dragged along with each eye movement, renders the system overdamped. The increase in viscous force, especially at high (saccadic) velocities, significantly impacts the system dynamics [8].

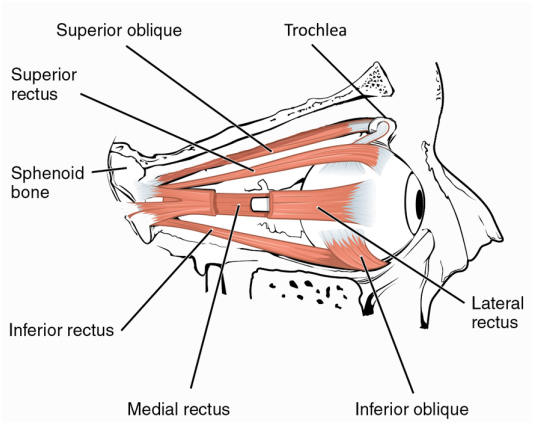

Fig. 1. Representation of the right human eye with the six extra-ocular muscles around it (to visualize medial rectus, lateral rectus is partially cut from view). Image adapted from [9] and shared under CC BY 4.0 license.

III. State of the Art

Most robotic eyes in the literature have been developed for the purpose of active visual perception tasks or human-robot interactions [10]–[16]. Therefore, their actuation mechanisms often focused on physical performance rather than on biological realism. The most common models are equipped with belts, or direct motor-driven cameras for incorporating pan-and-tilt rotations [10], [13]. A couple of models also use tendon-driven mechanisms [11], [12], flexible links [17], or magnetic coils [16] to control the pan-and-tilt motion. A small number of robotic eyes do have 3 Degrees of Freedom (DoF) which are driven by parallel links [14], motorized gimbals [15] or rotating frictional pads [18].

However, only a few models have been created based on biologically inspired actuation with the aim of better understanding the human oculomotor system and its behavior. Table III gives a comparative overview of these robotic eyes. The MAC-Eye [19] is a cable-driven robotic eye with four cables that are actuated by motors. They implement Listing's Law by mechanically restricting the cables to predetermined routing paths. In this way, the system was constrained to 2 DoF for all its rotations. It should be noted, however, that Listing's Law only holds for voluntary eye movements with the head upright and still, and the eyes looking at infinity. It is modified for near-viewing [25] and violated during vestibular-induced and optokinetic eye movements [26], as well as during combined eye-head gaze shifts [27]. Since MAC-Eye can't violate Listing's Law because of the physically imposed constraint, it doesn't help understand how this property emerges in humans.

To model more biologically realistic eye muscles, Rajendran et al. [20] used four contractile super-coiled polymer (SCP) muscles with a high power-to-weight ratio in their robotic eye. Like its biological counterpart, the SCP muscle contracts upon activation. They used it to control the eye in 2 DoF with a learning-based controller. Wang et al. [21] equipped their robotic eye with six pneumatic artificial muscles to move the eye in 3 DoF. Though both of these works focus on using more human-like muscles, they disregard the asymmetry of the human eye muscles and don't implement realistic muscle paths. They both also did not generate realistic saccade-like movements.

TABLE I
Pulling actions of muscles on the right eye

Muscle	Action
Superior rectus	Elevates, adducts, inward cyclo-torsion
Inferior rectus	Depresses, adducts, outward cyclo-torsion
Lateral rectus	Abducts
Medial rectus	Adducts
Superior oblique	Abducts, depresses, inward cyclo-torsion
Inferior oblique	Abducts, elevates, outward cyclo-torsion

TABLE II
Muscle insertion by Miller et al. [6]

	MR	LR	SR	IR	SO	IO
Origin						
x (mm)	-17.00	-13.00	-15.00	-17.00	-18.00	-13.00
y (mm)	-30.00	-34.00	-31.76	-31.76	-31.50	10.00
z (mm)	1.00	-1.00	3.60	-2.40	5.00	-15.46
Insertion						
x (mm)	-9.65	10.08	2.76	1.76	2.90	8.00
y (mm)	8.84	6.50	6.46	6.85	-8.00	-9.18
z (mm)	0.00	0.00	10.25	-10.22	8.82	0.00

TABLE III
STATE OF ART CABLE/MUSCLE-DRIVEN ROBOTIC EYES.

Robotic Eye	Joint Type	Muscles	Muscle type	Realistic muscle direction	Eye movement DoF	Features
MACEYE [19]	Supported sphere	4	Cables with motors	✗	2	Constrained muscle paths to implement Listing's Law
Rajendran et al. [20]	Ball & socket	4	Contractile SCP muscles	✗	2	2D positioning with learning-based control
Wang et al. [21]	Ball & socket	6	Pneumatic muscles	✗	3	Focus on construction and calculations of muscle lengths
Lakzadeh, M. [22]	Gimbal	6	Cables with motors	✓	3	3D orientation control and 1D saccades
John et al. [23]	Ball & socket	6 (3 input)*	Cables with motors	✓	3	Show emergence of saccadic properties from optimal control

* The robot in [24] has a rod connected to each motor and the cable pairs are attached to the ends

The system developed by Lakzadeh et al. [22] used 6 cables with motors, incorporating accurate insertions and pulling directions. They used a 3 DoF orientation-based controller to perform 1D saccades. However, there is a small caveat to their model, the joint of the eyeball was made with a gimbal. This changes the inertia of the eyeball while moving and makes it ineffective for studying the dynamic properties of saccades in full 3D.

We recently analyzed the 3D properties of saccades generated by a physics-derived simulator of a 3 DoF cable-driven prototype of a robotic eye [23]. The insertion points of the elastic cables were in close agreement with those of the human eye, whereas the six cables were coupled by a connecting rod as three antagonistic pairs, each pair actuated by its own motor. An optimal control algorithm that minimized a total cost function was used to produce realistic saccades across the full oculomotor range of the system in accordance with Listing's Law.

However, despite these promising results, the model was incomplete in several respects: first, the prototype was prone to vibrations and had low dynamic viscosity. Second, the hard-wired agonist-antagonistic coupling in the system did not do justice to the fact that in the human brain each eye muscle is controlled by its own driving signal. We here present and test a novel design that overcomes these problems.

IV. Design criteria

The major goal of our work is to create a robotic eye to help understand how the brain programs saccades by controlling the six extraocular muscles for each eye. Here, we present a model for the right eye. The core features of our new design are as follows:

1) A spherical eyeball, with camera and IMU, and unconstrained 3D rotational freedom around a fixed point.
2) Six independently controllable cables with realistic pulling directions.
3) High dynamic damping.

In addition to this, we wanted to keep the inertia of the eye as low as possible and make the design with future miniaturization in mind.

V. Design and implementation

The eye is encased in a cuboid box ('the head') with two sides open and a circular opening in the front (see Fig. 2). Details of the design and the components used are explained below.

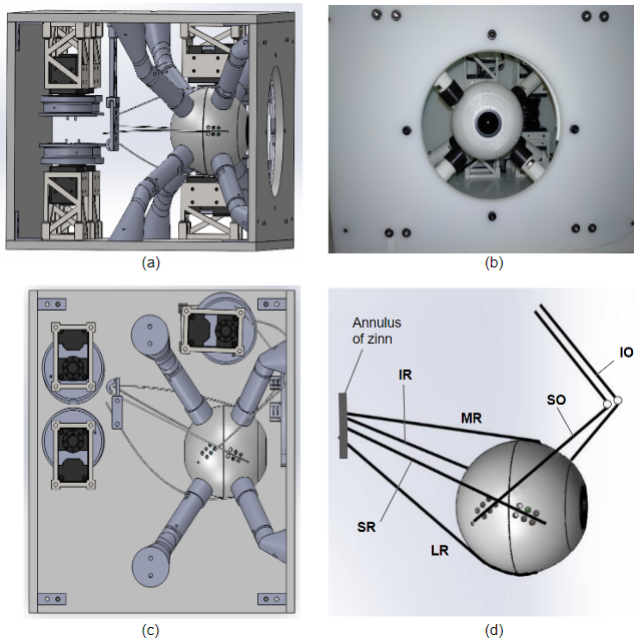

Fig. 2. (a) 3D CAD model of the robotic eye with six motors (four in the back and two hidden from view behind the eye) independently controlling the six cables connected to the eyeball. The eye is kept in place by eight spring-loaded supports with ball rollers to enable unconstrained 3D rotations around its fixed center. (b): Front view of the finished mechanical prototype showing the eye with the camera. (c) Top view of the CAD model. (d) Figure showing the muscle directions.

A. Eyeball

A spherical eyeball (8 cm diameter) was 3D printed with ABS filament. It is composed of a front and back part to allow the installation of an IMU and an IDS Imaging uEye camera. The data cables for the IMU and camera pass through an opening at the back. A spherical cover is placed on the front for aesthetic reasons. Figure 3 shows the exploded view of the eyeball and its components. The insertion points of the human

eye muscles (Table II) were scaled up and replicated on the robot's eyeball. Additional holes along the cable direction are made for future experimentation with cable routing.

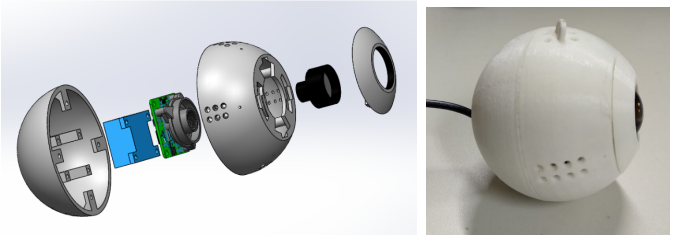

Fig. 3. Left: Exploded view of the CAD model of the eyeball with the IMU, camera and lens. Right: Side view of the final eyeball showing the holes for potential cable insertion point.

B. Eyeball Support

The support mechanism for the eyeball had to accommodate the asymmetric and changing directions (with eye movements) of the cables around the eye. At the same time, static friction should be small, while dynamic viscous damping must be sufficiently high. Therefore, we designed eight spring-loaded rollers, positioned such that interference with the cables was avoided, and the eye was kept fixed in space, while it had full 3D rotational freedom (Fig. 4). To provide sufficient damping during eye rotations, the rollers were lubricated with a high-viscosity lubricant.

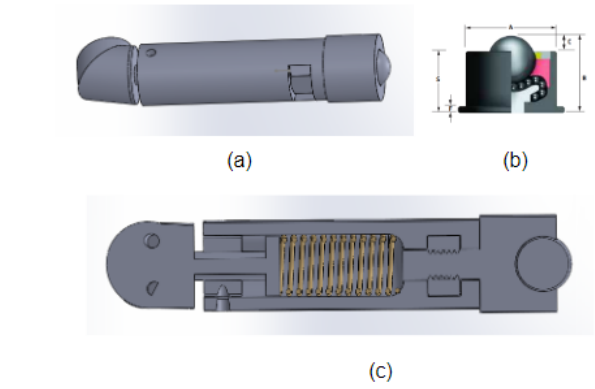

Fig. 4. (a) A CAD model of one spring-loaded support. (b) Rollers used for the support. (c) Cross-sectional view showing spring and piston inside the support.

C. Actuation

The eye muscles were represented by 0.3 mm diameter nylon wires, which provide low friction and very little stretch. One end of each cable was attached to a muscle insertion point on the eye, and subsequently routed, to their respective head-fixed insertion points (the routing points before the cables reach the motor). Since the Superior Oblique (SO) muscle passes through the trochlea, that was taken as the head-fixed insertion point for that muscle to simplify construction. Figure 2 (d) shows a top view of the eyeball with the different cable directions.

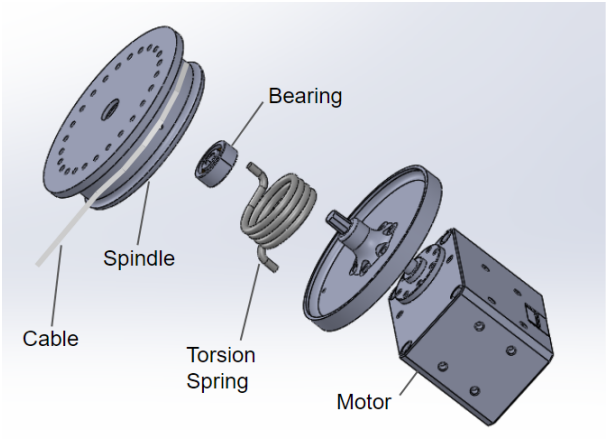

Fig. 5. Exploded view of a motor and spindle system with a torsional spring coupling them.

The cables can be independently actuated by six Dynamixel XM430-W210-R motors which were selected to balance torque and speed requirements. The four motors actuating the recti cables were placed at the back of the box, while the motors for the two obliques were placed on the side. One end of a cable was wrapped around a spindle/pulley (Fig. 5), such that rolling the spindle would pull the cable and make the eye move. To provide elasticity to the cables we decoupled the spindle from the motor with a ball bearing and incorporated a torsion spring between them. The spindle rotation at the start could be adjusted to set the initial cable lengths, and hence the muscle pretensions on the eyeball.

VI. Modeling and Simulation

In order to speed up the experimentation with the design, we modeled the physics of the system and simulated it. The eye was modeled as a sphere with a fixed center, subject to Newton-Euler's rigid body equation of angular motion:

$$ {}^{e}\boldsymbol{\alpha}_{h,e} = {}_{e}\mathbf{I}_{e}{}^{-1}({}_{e}\boldsymbol{\tau}_{net}(\boldsymbol{x},\boldsymbol{u}) - {}^{e}\boldsymbol{\omega}_{h,e} \times {}_{e}\mathbf{I}_{e}\,{}^{e}\boldsymbol{\omega}_{h,e}) \quad (1) $$

where ${}^{e}\boldsymbol{\alpha}_{h,e}$ is the angular acceleration of the eye with respect to the head frame, expressed in the eye frame; ${}_{e}\mathbf{I}_{e}$ represents the inertia tensor of the eye model;${}_{e}\boldsymbol{\tau}_{net}$ is the net torque exerted on the eye; $\boldsymbol{u}$ is the motor configuration of the 6 motors; ${}^{e}\boldsymbol{\omega}_{h,e}$ is the angular velocity of the eye and the symbol '$\times$' denotes the vector cross product.

The net torque is the sum of the elasticity and dynamic friction torques, ${}_{e}\boldsymbol{\tau}_{k}$ and ${}_{e}\boldsymbol{\tau}_{d}$, respectively:

$$ {}_{e}\boldsymbol{\tau}_{net} = {}_{e}\boldsymbol{\tau}_{k} + {}_{e}\boldsymbol{\tau}_{d} = \sum_{m=1}^{6} {}_{e}\boldsymbol{\tau}_{m} - \mathbf{D}_{eye}\,{}^{e}\boldsymbol{\omega}_{h,e} \quad (2) $$

where $\mathbf{D}_{eye}$ is the damping matrix, subscript m is the motor index ($m \in \{IR, MR, SR, LR, IO, SO\}$), and ${}_{e}\boldsymbol{\tau}_{m}$ is the torque exerted by each muscle. ${}_{e}\boldsymbol{\tau}_{m}$ can be computed with

$$ {}_{e}\boldsymbol{\tau}_{m} = {}^{e}\mathbf{P}_{m} \times {}_{e}\mathbf{f}_{m} \quad (3) $$

where ${}^{e}\mathbf{P}_m$ is each muscle's insertion point on the eye in the eye frame, and ${}_{e}\mathbf{f}_m$ is the tension force applied by each muscle on the eyeball.

The nylon cable along with the torsional spring can be approximated as an elastic linear elastic spring. So the elastic force applied by each muscle on the eye, ${}_{e}\mathbf{f}_m$, depends on its length (l_m), which is the sum of the cable length wound on the motor spindle and the length between the head-fixed routing point (represented by the white points in Fig. 6) and the eye-fixed insertion point (red points). The length of the cable for each muscle (l_m) varies with the rotation of the motors ($\mathbf{u}$) and orientation of the eye $\boldsymbol{x}$; (we omit time index t, for clarity),

$$l_m(\mathbf{x}, \mathbf{u}) = \left\| {}^{h}\mathbf{P}_{eye,m}(\mathbf{x}) - {}^{h}\mathbf{P}_{head,m} \right\| + r \cdot u_m \qquad (4)$$

where ${}^{h}\mathbf{P}_{eye}$ and ${}^{h}\mathbf{P}_{head}$ are the insertion points of cable m in the head reference frame, r is the radius of the spindle, and u_m is the rotation angle of the spindle for cable m. So the elastic force given by Hooke's law is :

$${}_{e}\mathbf{f}_m = k(l_m(\mathbf{x}, \mathbf{u}) - l_{0m})\, {}_{e}\vec{\boldsymbol{\phi}}_{\boldsymbol{m}} \qquad (5)$$

where k is the approximated spring constant and l_{0m} is the length of cable m when it is not stretched. The direction of the force applied to the eye is represented by ${}_{e}\vec{\boldsymbol{\phi}}_{\boldsymbol{m}}$.

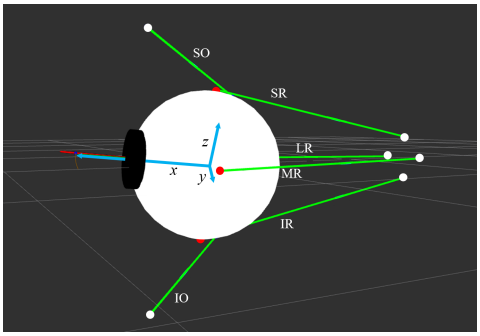

Fig. 6. Visualization of the extra-ocular muscles (green lines) for the simulator of our robotic eye. Here, its orientation deviated from the straight-ahead origin (indicated by the light blue axes) to the right (red line protruding from the pupil). Red and white dots indicate cable insertion points on the eye and on the head, respectively.

The simulation of the system was done in MATLAB and a graphical interface (Shown in Fig. 6) was made to visualize it.

VII. Experimental Results

We performed some tests to check the performance of the constructed robotic eye prototype, in particular the range of motion and the dynamic properties that make it suitable for our study of eye movements. Angular displacements of the eye were measured with the IMU during dynamic movement. However, as the IMU presents some drift, absolute orientations were measured using the image information with the help of markers in the field of view.

To measure the oculomotor range we performed movements of the motors from the rest position towards the periphery while keeping the cables' tensions under reasonable limits. We were able to make movements in the following ranges from a straight-ahead orientation without any issues:

- Horizontal : $\pm$ 55 degrees.
- Vertical : $\pm$ 40 degrees.
- Torsional : $\pm$ 30 degrees.

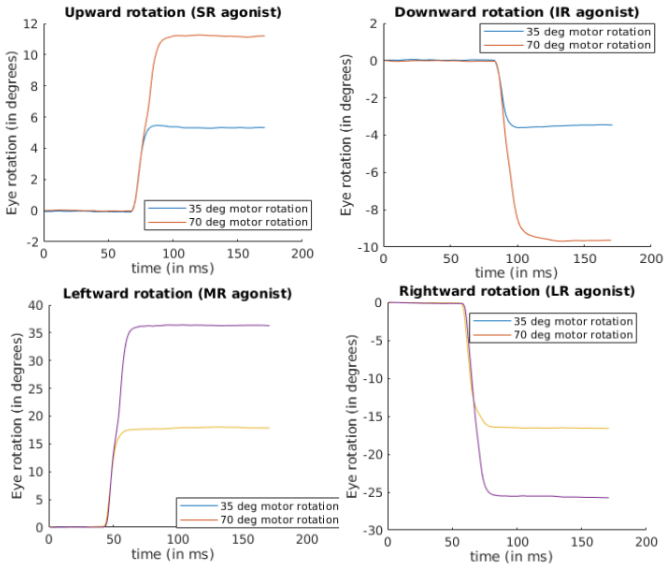

Fig. 7. Step responses for two different motor amplitudes in horizontal and vertical eye movement directions, done by coupling one pair of agonist and antagonist motors. As can be seen in the figures, the response is not linearly scaled and is direction-dependent due to the non-linearity and asymmetry in the system.

For understanding the dynamic response of the system we performed step inputs with different amplitudes and directions. For this, we coupled the agonist and antagonist motors by giving a positive step to the agonist motor and a negative step to the antagonist motor. The results are shown in Figure 7. There doesn't seem to be any significant overshoot or vibrations in any of the cases. The rise times of the responses are very short (a few tens of milliseconds) which makes it feasible to implement a wide range of ocular movements, including saccades. The response is not linearly scaled and comparing the figures it is also evident that the response is direction dependent because of the asymmetry of the muscles. For the same motor rotation, there is a large movement in the horizontal direction than the vertical one because the horizontal cables like the human muscles almost fully act in the horizontal plane while the others are more coupled in their pulling directions.

VIII. Conclusion

This paper has proposed a design for a cable-driven bio-inspired robotic eye for studying oculomotor control and understanding how the stereotypical properties of saccadic eye movements come about in the highly non-linear eye plant. The robot has a good range of achievable orientations and has enough damping to prevent overshoot. The proposed model also incorporated, for the first time, 6 independently controlled

muscles with realistic muscle paths and provides an effective testbed to study both orientation and dynamic properties of eye movements in full 3 DoF.

In future work, we plan to find methods to increase the rotational damping of the system to make it overdamped and use optimal control to understand how humanlike eye movement characteristics might emerge in this robotic system. Using the camera built into the eye we also plan to study how the characteristic saccadic properties might influence the performance of visual tasks with foveated vision.

ACKNOWLEDGMENT

This research was supported by the LARSyS - FCT Project (UIDB/50009/2020), VOAMAIS (PTDC/EEI-AUT/31172/2017, 02/SAICT/2017/31172), and the European Commission project ORIENT (ERC/2016/693400).

REFERENCES

[1] K. Hepp and V. Henn, "Iso-frequency curves of oculomotor neurons in the rhesus monkey," *Vision Research*, vol. 25, no. 4, pp. 493–499, 1985.

[2] F. C. Donders, "The 11th yearly report of the netherlands hospital for necessitous eye patients." Van de Weijer PW. Utrecht, the Netherlands, Tech. Rep., 1870, (in Dutch).

[3] A. T. Bahill, M. R. Clark, and L. Stark, "The main sequence: a tool for studying human eye movements," *Mathematical Biosciences*, vol. 24, pp. 191–204, 1975.

[4] R. J. Leigh and D. S. Zee, *The neurology of eye movements*. Oxford University Press, 5th ed., 1085 pages, 2015.

[5] D. A. Robinson, "Modeling the oculomotor control system," *Progress in Brain Research*, vol. 267, pp. 1–435, 2022.

[6] J. M. Miller and D. A. Robinson, "A model of the mechanics of binocular alignment," *Computers and Biomedical Research*, vol. 17, no. 5, pp. 436–470, 1984. [Online]. Available: https://www.sciencedirect.com/science/article/pii/0010480984900120

[7] J. L. Demer, "Current concepts of mechanical and neural factors in ocular motility," *Current Opinions in Neurology*, vol. 19, pp. 4–13, 2006.

[8] D. A. Robinson, "The mechanics of human saccadic eye movement," *Journal of Physiology*, vol. 174, pp. 245–264, 1964.

[9] J. G. Betts *et al.*, *Anatomy and Physiology*. OpenStax, 2013. [Online]. Available: https://openstax.org/books/anatomy-and-physiology/pages/1-introduction

[10] R. Beira, M. Lopes, M. Praca, J. Santos-Victor, A. Bernardino, G. Metta, F. Becchi, and R. Saltaren, "Design of the robot-cub (icub) head," in *Proceedings 2006 IEEE International Conference on Robotics and Automation, 2006. ICRA 2006.*, 2006, pp. 94–100.

[11] S. Schulz, S. M. Borgsen, and S. Wachsmuth, "See and be seen – rapid and likeable high-definition camera-eye for anthropomorphic robots," in *2019 International Conference on Robotics and Automation (ICRA)*, 2019, pp. 2524–2530.

[12] Kyung-Geune Oh, Chan-Yul Jung, Mun-Taek Choi, and Seung-Jong Kim, "Eye motion generation in a mobile service robot 'silbot ii'," in *2010 IEEE Workshop on Advanced Robotics and its Social Impacts*, 2010, pp. 59–64.

[13] D. Dansereau, D. Wood, S. Montabone, and S. B. Williams, "Exploiting parallax in panoramic capture to construct light fields," in *ICRA 2014*, 2014.

[14] H. Liu, J. Luo, P. Wu, S. Xie, and H. li, "Symmetric kullback-leibler metric based tracking behaviors for bioinspired robotic eyes," *Applied Bionics and Biomechanics*, vol. 2015, pp. 1–11, 11 2015.

[15] D. Fan, X. Chen, T. Zhang, X. Chen, G. Liu, H. M. Owais, H. Kim, Y. Tian, W. Zhang, and Q. Huang, "Design of anthropomorphic robot bionic eyes," in *2017 IEEE International Conference on Robotics and Biomimetics (ROBIO)*, 2017, pp. 2050–2056.

[16] A. Heya, Y. Nakata, H. Ishiguro, and K. Hirata, "Two-degree-of-freedom actuator for robotic eyes," in *2020 International Conference on Electrical Machines (ICEM)*, vol. 1, 2020, pp. 735–740.

[17] Y.-C. Lee, C.-C. Lan, C.-Y. Chu, C.-M. Lai, and Y.-J. Chen, "A pan–tilt orienting mechanism with parallel axes of flexural actuation," *IEEE/ASME Transactions on Mechatronics*, vol. 18, pp. 1100–1112, 2013.

[18] C. Huang, J. Gu, J. Luo, H. Li, S. Xie, and H. Liu, "System design and study of bionic eye based on spherical ultrasonic motor using closed-loop control," in *2013 IEEE International Conference on Robotics and Biomimetics (ROBIO)*, 2013, pp. 2685–2690.

[19] G. Cannata and M. Maggiali, "Models for the design of bioinspired robot eyes," *IEEE Transactions on Robotics*, vol. 24, no. 1, pp. 27–44, 2008.

[20] S. K. Rajendran, Q. Wei, and F. Zhang, "Two degree-of-freedom robotic eye: Design, modeling, and learning-based control in foveation and smooth pursuit," *Bioinspiration biomimetics*, vol. 16, 05 2021.

[21] X. yin Wang, Y. Zhang, X. jie Fu, and G. shan Xiang, "Design and kinematic analysis of a novel humanoid robot eye using pneumatic artificial muscles," *Journal of Bionic Engineering*, vol. 5, no. 3, pp. 264–270, 2008. [Online]. Available: https://www.sciencedirect.com/science/article/pii/S1672652908600347

[22] M. Lakzadeh, "A biologically-inspired eye model for testing oculomotor control theories," Master's thesis, University of British Columbia, 2012. [Online]. Available: https://open.library.ubc.ca/collections/ubctheses/24/items/1.0072549

[23] A. John, C. Aleluia, A. J. Van Opstal, and A. Bernardino, "Modelling 3d saccade generation by feedforward optimal control," *PLOS Computational Biology*, vol. 17, no. 5, pp. 1–35, 05 2021. [Online]. Available: https://doi.org/10.1371/journal.pcbi.1008975

[24] M. R. C. Lucas, "Construction and Characterization of a Biomimetic Robotic Eye Model with Three Degrees of Rotational Freedom: A Testbed for Neural Control of Eye Movements," Master's thesis, University of Lisbon, 2017.

[25] A. W. Minken and J. A. M. Van Gisbergen, "Dynamical version–vergence interactions for a binocular implementation of donders' law," *Vision Research*, vol. 36, no. 6, pp. 853–867, 1996.

[26] D. E. Angelaki and B. J. M. Hess, "Control of eye orientation: where does the brain's role end and the muscle's begin?" *European Journal of Neuroscience*, vol. 19, no. 1, pp. 1–10, 2004. [Online]. Available: https://onlinelibrary.wiley.com/doi/abs/10.1111/j.1460-9568.2004.03068.x

[27] D. Tweed, B. Glenn, and V. T, "Eye-head coordination during large gaze shifts," *Journal of Neurophysiology*, vol. 73, no. 2, pp. 766–779, 1995.